CHEMISTRY OF MATERIALS

Article

pubs.acs.org/cm

Computational Discovery of Hydrogen Bond Design Rules for Electrochemical Ion Separation

Terry Z. H. Gani, Efthymios I. Ioannidis, and Heather J. Kulik*

Department of Chemical Engineering, Massachusetts Institute of Technology, Cambridge, Massachusetts 02139, United States

Supporting Information

ABSTRACT: Selective ion separation is a major challenge with far-ranging impact from water desalination to product separation in catalysis. Recently introduced ferrocene (Fc)/ferrocenium (Fc^+) polymer electrode materials have been demonstrated experimentally and theoretically to selectively bind carboxylates over perchlorate through weak C−H···O hydrogen bond (HB) interactions that favor carboxylates, despite the comparable size and charge of the two species. However, practical application of this technology in aqueous environments requires further selectivity enhancement. Using a first-principles discovery approach, we investigate the effect of Fc/Fc^+ functional groups (FGs) on the selectivity and reversibility of formate−Fc^+ adsorption with respect to perchlorate in aqueous solution. Our wide design space of 44 FGs enables identification of FGs with higher selectivity and rationalization of trends through electronic energy decomposition analysis or geometric hydrogen bonding analysis. Overall, we observe weaker, longer HBs for perchlorate as compared to formate with Fc^+. We further identify Fc^+ functionalizations that simultaneously increase selectivity for formate in aqueous environments but permit rapid release from neutral Fc. We introduce the materiaphore, a 3D abstraction of these design rules, to help guide next-generation material optimization for selective ion sorption. This approach is expected to have broad relevance in computational discovery for molecular recognition, sensing, separations, and catalysis.

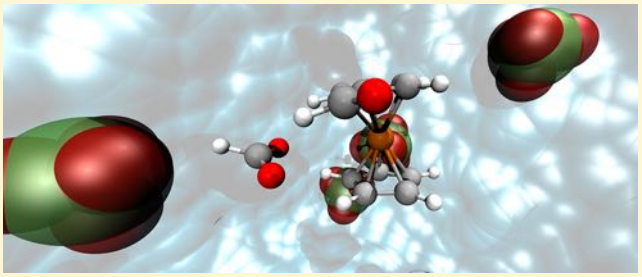

1. INTRODUCTION

The removal of ions from solution is a crucial challenge with applications ranging from water desalination,[1] wastewater treatment,[2] and capture of valuable metals from seawater[3] to product separation in homogeneous catalytic processes.[4] At present, the commonly used methods of distillation,[5] sorption,[3] and filtration[1] are energy-inefficient, slow, or expensive. Formate is a major product of photochemical,[6] biological[7] and electrochemical[8] CO_2 reduction, and its in situ capture could potentially play a role in integrated liquid-based CO_2 capture and hydrogen storage technologies.[9,10] Hence, the development of low-cost and energy-efficient methods for separating ions such as formate would not only significantly reduce carbon emissions and energy costs but also provide new routes to useful chemicals.[11] However, selective recovery of ions from solution is particularly challenging due to high similarity in shape and charge.[12]

Electrochemical separations of charged from neutral species via Coulombic attraction have demonstrated promise due to their switchability, speed, and energy-efficiency.[13−16] The reversible one-electron oxidation of ferrocene (Fc) to ferrocenium (Fc^+) renders it suitable for a wide range of electrochemical applications,[17−19] and recently a Fc/Fc^+-based redox system consisting of polyvinyl(ferrocene) polymer adsorbed on a carbon nanotube electrode was shown to reversibly and selectively bind carboxylates (e.g., formate) over other ions (e.g., perchlorate) in organic solvent 3000-fold and aqueous solution 140-fold.[16] Although the aqueous solution separation ratio in water is impressive considering the strong electrostatic screening due to water's large dielectric constant (ca. ε = 80 at room temperature), practical aqueous separation in typical applications mandates further improvement in selectivity. The different affinities of Fc^+ for the two anions despite comparable size and charge suggests more complex interactions than pure Coulombic attraction,[20−23] and density functional theory (DFT) calculations preliminarily attributed[16] the selectivity to differences in hydrogen bond (HB) strengths of anions to Fc^+.

Strong, directional hydrogen bonding is a key paradigm in selective anion recognition,[12,24−27] catalysis,[28−32] drug design,[33−36] and materials design.[37−39] In anion recognition in particular, HB donors distributed uniformly around a cavity of desired size[12,24,40,41] have been shown to be suitable for size-selective sensing of symmetric anions, whereas shape-selective sensing is achieved via orienting the same strong HB donors to match locations of HB acceptors in the target anion.[12,24,26,27,42] Typical strong HB donors employed include amides/amines[12,24−27] and triazoles.[27] Many of these designs have incorporated the Fc moiety due to the ease of functionalization[24,26,43] of its rigid sandwich structure, albeit binding at the

Received: June 13, 2016
Revised: August 22, 2016
Published: August 22, 2016

DOI: 10.1021/acs.chemmater.6b02378
Chem. Mater. 2016, 28, 6207−6218

HB donor, not proximal to the Fc core. The structure and properties of unsubstituted[44] and substituted[45,46] Fc and Fc^+ have also been investigated with computational DFT studies. Additionally, redox-selective sensors[24,26,47,48] have been created based on the reversible one-electron oxidation of Fc typically accompanied by irreversible binding, although reversible adsorption is required for separations.[16]

The central importance of HBs in materials design and fundamental chemistry has motivated development of classical electrostatic models[27,49,50] and empirical correlations,[50−52] whereas first-principles computational modeling is crucial to the continued development of understanding hydrogen bonding.[53−55] In response to recent experimental and theoretical advances, the International Union of Pure and Applied Chemistry recently broadened the HB[56] definition to be "an X−H···Y interaction where X is more electronegative than H and there is sufficient evidence of H···Y bond formation". Of particular interest to the selective sorption of anions at Fc^+ is the weak hydrogen bond, a class of HBs where the HB donor and/or acceptor is of moderate to low electronegativity.[57−59] C−H···O HBs, better known in structural biology,[59,60] were recently implicated[16] through combined computational and experimental study to be key for selective carboxylate adsorption with Fc^+. Although initially thought to be indistinguishable from van der Waals forces,[61,62] extensive crystallographic[57−59,63] and computational[64,65] evidence of C−H···O strength and directionality has reclassified C−H···O interactions as weakly directional HBs.[59] We thus hypothesize that the Fc^+ core can be functionalized to further improve selectivity for anion separation in aqueous solutions while maintaining weak reversible adsorption by tuning strength and numbers of C−H···O interactions.

DFT-based computational screening has become an increasingly valuable tool for the design and discovery of new materials[66−71] thanks both to recent improvements in computational efficiency and accuracy (e.g., in descriptions of intermolecular forces through direct treatment of dispersion[72,73]). In this work, we carry out the first computational screen to identify design strategies for Fc^+ core functionalization to maximize formate selectivity and reversibility in the Fc/Fc^+ redox system. The rest of the manuscript is outlined as follows. In Section 2, we summarize the Computational Details of our simulations. In the Results and Discussion (Section 3), we rationalize the electronic structure factors driving selective, reversible formate adsorption across our design space and summarize ideal materials properties. In Section 4, we provide our Conclusions.

2. COMPUTATIONAL DETAILS

First-Principles Calculations. Initial electronic structure calculations, including single point energies and geometry optimizations, were carried out using the TeraChem[74,75] graphical processing unit (GPU)-accelerated quantum chemistry package with the B3LYP[76−78] hybrid exchange-correlation functional. The default definition of B3LYP in TeraChem employs the VWN1-RPA form for the LDA VWN[79] component of LYP[76] correlation. Iron, bromine, and iodine were treated with the LANL2DZ effective core potential,[80] and the 6-31G* basis was used for the remaining atoms. Results were found to be generally insensitive to basis set size (see Supporting Information Table S1 and Figure S1). Fc^+ cores were simulated with a +1 charge and doublet spin multiplicity, and all Fc^+−anion complexes were simulated with a neutral total charge and doublet spin multiplicity. Reduced Fc structures and complexes were assigned an additional −1 charge and simulated as singlets. Both Fc^+ and Fc calculations were spin-unrestricted with virtual and open-shell orbitals level-shifted[81] by 1.0 and 0.1 eV, respectively, to aid self-consistent field (SCF) convergence to an unrestricted solution. Dispersion interactions were modeled by augmenting B3LYP with the empirical DFT-D3 correction.[72] Selected comparisons using the long-range corrected hybrid exchange-correlation functional ωPBEh[82] were also carried out (Supporting Information Table S2). The aqueous solvent environment was modeled using an implicit polarizable continuum model (PCM) with the conductor-like solvation model (COSMO[83,84]) and ε = 78.39. The solute cavity was built using Bondi's van der Waals radii[85] scaled by a factor of 1.2 for available elements and a custom radius of 2.05 Å for iron. The process of adsorption between formate or perchlorate and the FG−Fc^+ requires partial desolvation of either the formate or perchlorate ion and the associated FG−Fc^+. We address this desolvation contribution through our use of a polarizable continuum implicit solvent model. Near-chemical accuracy is achieved between our model of formate−perchlorate relative adsorption of 4 kcal/mol (2 kcal/mol with entropic contributions) with unfunctionalized Fc^+ and experimental value of 3 kcal/mol.[16] This agreement suggests beneficial cancellation of errors in the computed relative adsorption energies, which should be even stronger when comparing selectivity trends upon FG tuning (see Supporting Information Figure S2).

Structures. Geometry optimizations in the gas phase on molSimplify-generated[86] structures were carried out using the L-BFGS algorithm in Cartesian coordinates as implemented in DL-FIND.[87] For unfunctionalized Fc^+−anion adsorption studies, we employed the molSimplify additional molecule placement feature, which randomizes distance and orientation of the anion around the core Fc^+. The initial Fc^+−anion distance was constrained to be between 1 and 10 Å larger than the optimal distance between the two based on zero overlap between van der Waals radii. These unfunctionalized Fc^+ calculations were carried out with gas-phase optimization followed by a COSMO single point energy. For functionalized structures (FG−Fc^+) with an attached functional group (FG), COSMO optimizations were carried out on gas-phase-preoptimized structures.

For FG−Fc^+−anion adsorption studies, molSimplify was used to replace a hydrogen atom adjacent to the anion on the unfunctionalized, preoptimized Fc^+−anion "custom core" in the lowest energy adsorption mode (see Section 3a) with a new FG through the replace feature. The code aligns the new FG along the bond vector of the previously removed FG, assigns the new FG−core bond distance according to the sum of covalent radii, and performs predefined rotation routines to reduce steric repulsion. The custom core coordinates are provided in the Supporting Information (Table S3). This approach ensures maximum coincidence for the initial position of the ion across FGs and ensures evaluation of direct anion−FG interactions. Effects in the weaker, indirect adsorption configurations were also explored (Supporting Information Figure S3).

Analysis. Anion adsorption energies were calculated by subtracting the total electronic energies of optimized isolated Fc^+, $E_{(Fc^+)}$, and anion, $E_{(anion)}$, from the energy of the optimized anion/Fc^+ complex, $E_{(anion/Fc^+)}$:

$$\Delta E_{ads} = E_{(anion/Fc^+)} - E_{(Fc^+)} - E_{(anion)} \quad (1)$$

Basis set superposition error, as calculated with the counterpoise scheme,[88] was neglected after it was determined to be small and independent of the different FGs being compared. Similarly, zero point vibrational energy and entropic contributions to relative binding, as obtained from frequency calculations on gas-phase optimized geometries, were neglected due to small differences and negligible effect on any computed trends (Supporting Information Table S4 and Figure S4).

Natural bond orbital (NBO) partial charges were obtained from NBO analysis as implemented in the NBO v6.0 package[89] interfaced with TeraChem. Gas-phase absolutely localized molecular orbital-energy decomposition analysis (ALMO-EDA)[90] was performed in QChem 4.2[91] on TeraChem solvent-optimized geometries for all FG−Fc^+/anion pairs. ALMO-EDA decomposes the binding interaction into frozen density (FRZ), polarization (POL), and delocalization (DEL)

DOI: 10.1021/acs.chemmater.6b02378
Chem. Mater. 2016, 28, 6207−6218

terms and gives the charge transfer (CT) from the anion to Fc^+ in milli-electrons. The gas phase ALMO-EDA analysis with B3LYP overestimated the extent of charge transfer in some cases, as noted in the Results and Discussion, and these points were excluded from some analysis (see Supporting Information Table S2). The quantum theory of atoms in molecules (QTAIM) bond critical points (BCPs)[92] of all solvent-optimized anion−Fc^+ complexes were identified with the Multiwfn package.[93] As defined in ref 94, HB energies were estimated from the potential energy density (V) of the closest BCP to a putative HB:

$$E_{HB} = V(\mathbf{r}_{BCP})/2 \quad (2)$$

3. RESULTS AND DISCUSSION

3a. Anion Adsorption Modes. To identify the most stable adsorption mode between formate and Fc^+, we generated and geometry-optimized 100 formate−Fc^+ complex random initial configurations. The optimized structures may be grouped into six adsorption modes distinguished by (i) the distance of the formate center of mass (COM) to the Fc^+ iron and (ii) formate orientation (Figure 1). Four adsorption modes, similar to those

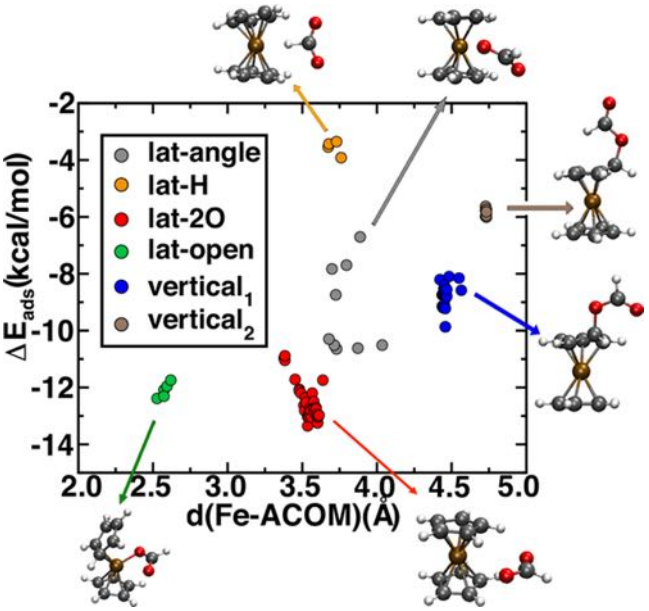

Figure 1. Adsorption energies (ΔE_{ads}, in kcal/mol) versus iron−anion center of mass distance (d(Fe-ACOM), in Å) for 100 formate−Fc^+ complexes. The data is clustered into 6 adsorption modes of formate on Fc^+: (i) an open lateral mode (lat-open, green circles), ii−iv) three closed lateral modes (lat-2O, red circles; lat-angle, gray circles; lat-H, yellow circles), and v−vi) two vertical modes ($vertical_1$, blue circles and $vertical_2$, brown circles).

that have been previously observed,[95] have a lateral formate with (i) open Fc^+ (centered at 2.5 Å, lat-open), closed Fc^+ with (ii) both oxygen atoms (3.5 Å, lat-2O), (iii) one oxygen (3.8 Å, lat-angle), or (iv) the hydrogen (3.7 Å, lat-H) atom oriented toward Fc^+. The closed Fc^+ adsorption modes have HBs between formate oxygen atoms and cyclopentadienyl (Cp^-) ring hydrogen atoms, whereas in the lat-open adsorption mode formate oxygen atoms directly coordinate the Fe center. Two vertical adsorption modes in which a formate binds to one of the Cp^- rings correspond to (v) both formate oxygen atoms oriented toward Fc^+ (4.5 Å, $vertical_1$) or (vi) one oxygen atom oriented away from Fc^+ (4.8 Å, $vertical_2$).

These six adsorption modes produce a wide range of solvent-screened ΔE_{ads} from −4 kcal/mol for the weakest (iv, lat-H) adsorption mode up to −14 kcal/mol for the strongest (ii, lat-2O). The relative ΔE_{ads} of the local minima depend only weakly on the formate−Fc^+ distance and are more sensitive to bonding variations: noncovalent interactions present in lat-angle, lat-H and lat-2O; C−O covalent bonding confirmed through NBO analysis for $vertical_1$ or $vertical_2$; and a 1.9 Å metal−ligand Fe−O bond for lat-open. The two lowest adsorption modes ca. −11 to −13 kcal/mol are (i) lat-open and (ii) lat-2O, and we expect the latter to be the dominant adsorption mode because opening the Fc^+ sandwich structure (Figure 1, bottom left) to produce lat-open is a strongly activated process involving breaking of multiple Fe−C π bonds. The vertical adsorption modes are significantly weaker due to disruption of Cp^- aromaticity, whereas the lat-angle and lat-H modes are less amenable for forming hydrogen-bonding interactions. We also geometry optimized 100 random initial configurations of perchlorate with Fc^+ and observed a single lateral adsorption mode with a narrow ΔE_{ads} distribution (−7 ± 0.5 kcal/mol). This single mode is consistent with perchlorate's symmetry, which prevents the formation of optimal, directional HBs, and its larger size that makes open binding unfavorable.

3b. Tuning Relative Formate−Perchlorate Selectivity. We hypothesize that formate and perchlorate ΔE_{ads} will be modulated differently through Fc^+ core functionalizations due to differences in the geometric and electronic properties of the anions (structures shown in Figure 2). A total of 44 different commonly employed FGs (Figure 3) of varied size, polarity and electron donating or withdrawing ability were included along with several FGs that have been experimentally synthesized for catalysis[96] (FGs **43** and **44**). The reduced 44 FG set was obtained after exclusion of 6 cases that did not converge to the most favorable lat-2O adsorption mode (Supporting Informa-

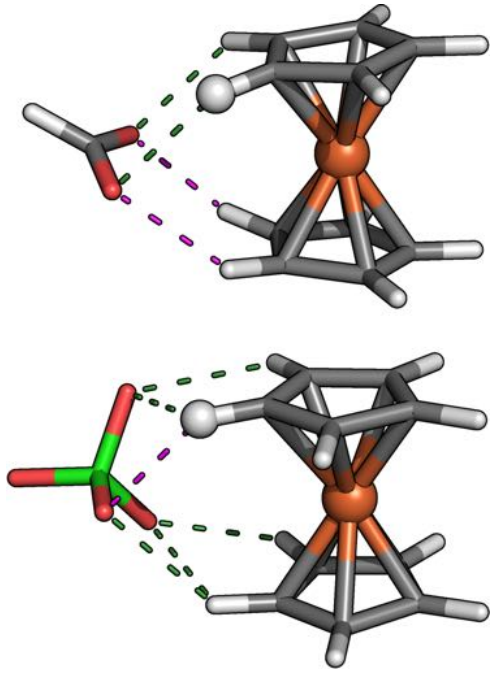

Figure 2. Anion complexation with unfunctionalized Fc^+. The attachment point for an FG is indicated by a white sphere. The magenta and green dashed lines represent short (<2.3 Å) and long (>2.3 Å) HBs, respectively.

DOI: 10.1021/acs.chemmater.6b02378
Chem. Mater. 2016, 28, 6207−6218

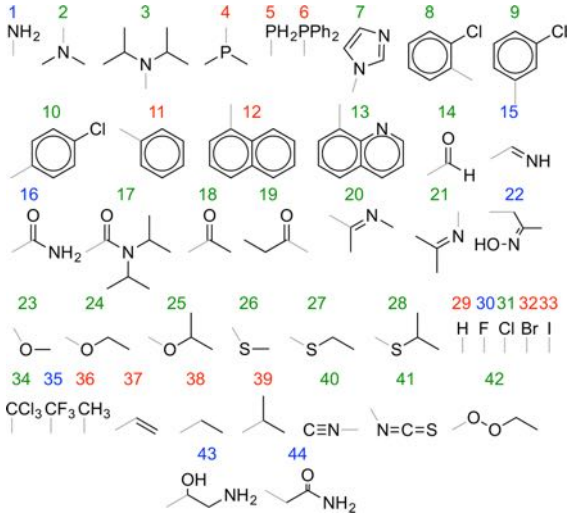

Figure 3. FGs in the computational screening data set. The connection to the Fc^+ core is denoted by a gray bond, and the colors of FG indices represent polar (blue), slightly polar (green), and nonpolar (red) character, as defined in the main text.

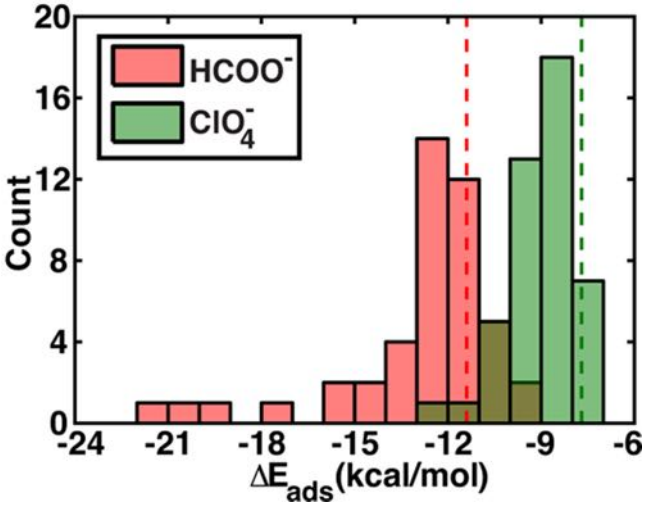

Figure 4. Histogram of ΔE_{ads} (in kcal/mol) for formate (red) and perchlorate (green) to FG−Fc^+ complexes. The dashed lines (red for formate, green for perchlorate) denote ΔE_{ads} for the unfunctionalized Fc^+. Formate shows a wider range of adsorption energies with FG−Fc^+ versus a narrower range for perchlorate.

tion Table S5). Acidic FGs were excluded from the set due to potential reaction with formate and the basicities in water of all FG−Fc^+s with known basic moieties were calculated and found to be negligible (Supporting Information Table S6). We then grouped the FGs by the largest difference in Pauling electronegativity (χ) between bonded atoms i and j:

$$\Delta\chi = \max|\chi_i - \chi_j| \quad (3)$$

Using this relative polarity metric, the 44 FGs may be divided into three roughly equally sized groups as (i) nonpolar: <0.4 (red, 14 FGs), (ii) slightly polar: 0.5 to 0.8 (green, 14 FGs), and (iii) polar: >0.8 (blue, 16 FGs) (all electronegativity values are provided in Supporting Information Table S7). For planar or highly asymmetric FGs (e.g., −CHO, **14** in Figure 3), we generated an additional structure with the anion on the opposite side and kept the lower energy complex after geometry optimization.

In the majority of cases, FGs strengthen both formate and perchlorate adsorption with respect to the pristine Fc^+, but formate has a wider range of ΔE_{ads} to FG−Fc^+s (−9 to −22 kcal/mol) than perchlorate (−7 to −13 kcal/mol), suggesting that it should be possible to enhance selectivity for formate over the pristine case (Figure 4). Indirect adsorption modes that would be preferred for anion/FG−Fc^+ complexes with ΔE_{ads} less than unfunctionalized Fc^+ were also considered but found to be less amenable to HB design compared to direct adsorption (see Supporting Information Figure S3). To identify FGs that tune Fc^+ selectivity for formate, we computed relative formate (f)/perchlorate (p) adsorption energies ($\Delta E_{ads}^{f\text{-}p}$):

$$\Delta E_{ads}^{f\text{-}p} = \Delta E_{ads}^{f} - \Delta E_{ads}^{p} \quad (4)$$

where values less than 0 denote stronger formate adsorption. Our screen produced 14 new FG−Fc^+ structures with increased formate selectivity over unfunctionalized Fc^+ ($\Delta E_{ads}^{f\text{-}p}$ = −4 kcal/mol) and a wide range (−11 to −1 kcal/mol) of relative selectivities. We identified that $\Delta E_{ads}^{f\text{-}p}$ is well-correlated to ΔE_{ads}^{f} with a linear best-fit (R^2 = 0.9):

$$\Delta E_{ads}^{f\text{-}p} = 0.66\Delta E_{ads}^{f} + 4.76 \text{ kcal/mol} \quad (5)$$

suggesting that formate selectivity can be increased by enhancing formate adsorption (Figure 5). Strongly polar FGs

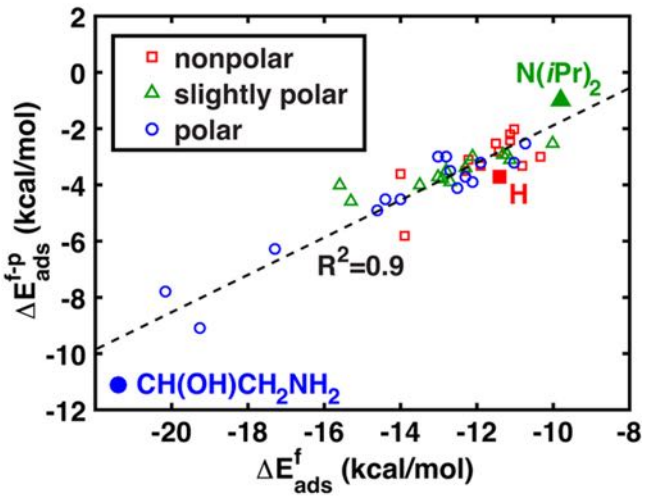

Figure 5. Relative formate−perchlorate adsorption energies ($\Delta E_{ads}^{f\text{-}p}$, in kcal/mol) versus corresponding formate adsorption energy (ΔE_{ads}^{f}, in kcal/mol) to FG−Fc^+. The black dashed line indicates a linear best-fit (R^2 = 0.9). FGs are grouped by polarity: nonpolar (red squares), slightly polar (green triangles), and polar (blue circles), as described in the main text. Annotated structures are indicated by larger, filled symbols.

such as **43** (alkanolamine, $\Delta E_{ads}^{f\text{-}p}$ = −11 kcal/mol), **44** (methyl amide), **16** (amide), and **1** (amine) (Figure 3) exhibit the strongest formate adsorption and, thus, formate selectivity, whereas bulky, nonpolar FGs such as diisopropylamine (**3**, $\Delta E_{ads}^{f\text{-}p}$ = −1 kcal/mol) are the weakest. To interpret subtler adsorption trends, we consider in detail the electronic and geometric properties of interactions in anion/FG−Fc^+ complexes.

3c. Intermolecular Interaction Analysis. Although anion−Fc^+ adsorption energies are due to both electrostatics and hydrogen bonding,[16] we hypothesize that FGs tune HB

DOI: 10.1021/acs.chemmater.6b02378
Chem. Mater. 2016, 28, 6207−6218

strength more than they alter electrostatics. To reveal HB strength, we begin by analyzing nonbonded distances between HB donors and acceptors in anion−Fc^+ complexes. We have selected a 3.0 Å H···O HB distance cutoff consistent with (i) the longest HBs for which QTAIM bond critical points (BCPs)[94] were detected in this work (Supporting Information Table S8) and (ii) the longest and weakest CH···O bonds observed experimentally.[57] Unfunctionalized Fc^+ forms two shorter CH···O bonds ca. 2.2 Å and two longer bonds ca. 2.4 Å with formate (Figure 2). The 3.5 Å height of Fc^+, as defined by the eclipsed H-to-H distance on the two Cp^- rings is too large to accommodate four short HBs to formate. To obtain four shorter, and presumably stronger, 2.2 Å HB distances, a less obtuse C−H···O angle of 127°, which is only observed experimentally for long, weak HBs,[57] would be required. In comparison to formate, perchlorate forms weaker but more numerous (6 in perchlorate vs 4 for formate) C−H···O bonds with unfunctionalized Fc^+. Despite a greater number of HBs, only one shorter 2.3 Å HB is observed, with the remaining 5 ranging from 2.4 to 2.6 Å.

Strong HB donors that form short HB distances are indeed a good indicator of FG−Fc^+ structures with high ΔE^{f}_{ads}. The strongest-binding FG, alkanolamine (**43**), forms an O−H···O HB with a 1.6 Å H···O distance between the alcohol H and the formate O (Figure 6), which is shorter than typical 1.7 to 2.0

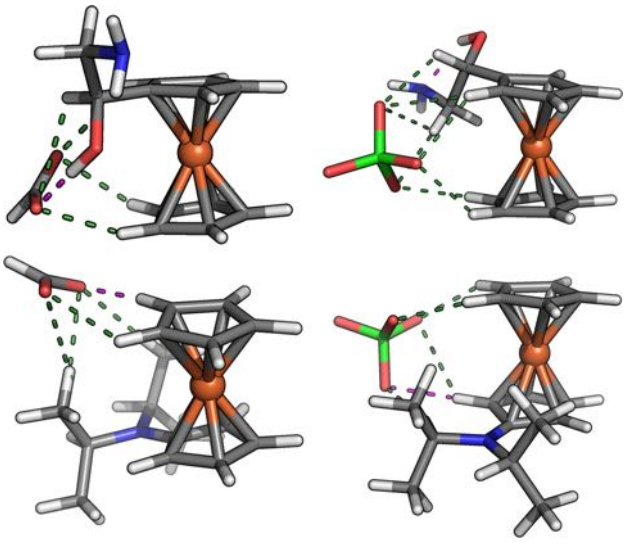

Figure 6. Hydrogen bonding interactions between (**43**) alkanolamine-functionalized Fc^+ and formate (top left) or perchlorate (top right) compared to (**3**) diisopropylamine-functionalized Fc^+ and formate (bottom left) or perchlorate (bottom right). The magenta and green dashed lines represent short (<2.3 Å) and long (>2.3 Å) HBs, respectively.

Å[97] H···O distances due to the negative charge on formate. In this complex, formate prefers an angled orientation to minimize distance to the HB donor on the FG rather than a lateral orientation preferred in pristine Fc^+. Beyond HB donor strength alone, more proximal HB donor placement is observed to strengthen formate adsorption and selectivity by introducing a third short, 135° HB without interrupting the short HBs to one Fc^+ Cp^- ring. Two notable examples of this effect are the methyl FG (**36**) and the isopropyl sulfide FG (**28**), in which formate ΔE_{ads} is increased by 1 and 3 kcal/mol, respectively, despite sp^3 HBs (i.e., the FGs) generally being much weaker than sp^2 HBs[50] (i.e., the Cp^- ring). Isopropyl sulfide (**28**) also strengthens ΔE^{f}_{ads} by altering formate orientation from lat-2O to a nearly perpendicular lat-angle adsorption mode in which a short 1.9 Å, nearly linear HB is formed between formate and the FG.

Alternatively, formate ΔE_{ads} can be lowered if the FG disrupts the strongly favorable formate−Cp^- interactions. The isopropyl hydrogen atom HB donors of the weakest binding and least selective FG, diisopropylamine (**3**) are too far away from the Fc^+ core (Figure 6). These FG HB donors pull formate away from the Fc^+ core (Fe to anion distance of 4.1 Å versus 3.5 Å in the unfunctionalized case), which simultaneously weakens HBs with Cp^- ring and reduces the distance-dependent electrostatic contribution to adsorption.

Consistent with the correlation between formate adsorption and selectivity (Figure 5), the specific FGs that strengthened formate adsorption do not strengthen perchlorate adsorption. For the strongest formate-binding FG (alkanolamine, **43**), there is no direct FG−perchlorate interaction, and the FG instead forms a 2.0 Å intramolecular O−H···N bond. Most of the 7 longer C−H···O HBs (2.3−2.7 Å) are instead between perchlorate and the FG ethyl chain. For the weak-formate binding FG (diisopropylamine, **3**), perchlorate's larger size enables interaction with the isopropyl hydrogen atoms through an additional 2.3 Å, 160 °C−H···O bond while maintaining HBs with Cp^-, strengthening the overall ΔE_{ads}. These extreme cases suggest (i) $\Delta E^{f\text{-}p}_{ads}$ is correlated to ΔE^{f}_{ads} because perchlorate forms weaker HBs with HB donors, and (ii) perchlorate selectivity is enhanced when its larger size forms HBs that formate cannot.

To generalize differences between formate and perchlorate adsorption to FG−Fc^+ structures, we examined the distributions of distances and angles in all HB interactions between the anions and Fc^+ structures (Figure 7). No HB angles below 100° were found for either anion, and the inverse correlation of long distances and small angles is consistent with the observation that dipole−monopole and dipole−dipole contributions to bond energies approach zero as the bond angle approaches 90°.[57] For formate, the HBs form a continuous band whereas for perchlorate, we instead observe distinct clusters. If one perchlorate oxygen atom occupies an optimal HB position (the middle cluster in Figure 7c), the other two coordinating oxygen atoms that form an equilateral triangle (side length 2.45 Å) with the first oxygen must then form weak, low-angle HBs, corresponding to the top left cluster. The third cluster arises from FG−Fc^+/perchlorate complex conformations in which one of the C−H···O bonds becomes almost linear. Individual HB distances are also shorter for formate than for perchlorate by ca. 0.1 Å even for the same angle. One-dimensional histograms of only HB angles (Figure 7a,b) reveal directionality for formate C−H···O bonds absent from perchlorate/Fc^+ complexes, consistent with weaker individual C−H···O interactions[58] for perchlorate. The greater numbers of HBs for perchlorate than formate appear substantially weaker by geometric analysis, suggesting further analysis of the relationship between HB distance ΔE_{ads}.

We thus correlated QTAIM[94]-derived HB energies with HB distance and angle and found a strong inverse-power correlation (R^2 = 0.99) with distance but only limited correlation with angle arising from the previously described angle−distance relationship (see Figure 7 and Supporting Information Table S8), consistent with previous HB characterization studies.[56,98−101] We use the inverse-power relationship

DOI: 10.1021/acs.chemmater.6b02378
Chem. Mater. 2016, 28, 6207−6218

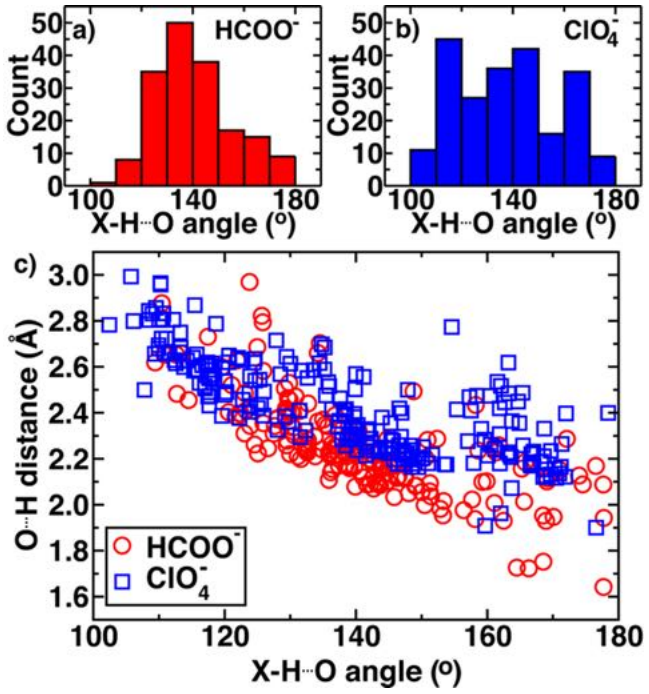

Figure 7. Hydrogen-bonding geometric properties: histogram of angles for (a) formate and (b) perchlorate as well as (c) scatterplot of angles (deg) versus O···H distances (Å) for HBs in functionalized Fc^+−formate (red circles) and Fc^+−perchlorate (blue squares) complexes.

between QTAIM HB energies and HB distance ($d_{O\cdots H}$) to introduce an HB score (HBS):

$$\mathrm{HBS} = 24.76(d_{O\cdots H})^{-5} \tag{6}$$

The HBS normalization constant was chosen by assigning a score of 1 to the strongest C−H···O bond in the data set ($d_{O\cdots H}$ = 1.9 Å). An overall anion/(FG)−Fc^+ complex HB score (CHBS) for each FG and anion is the sum of all HBS values over i HBs:

$$\mathrm{CHBS} = \sum_i \mathrm{HBS}_i \tag{7}$$

The CHBS excludes noncovalent intermolecular interactions other than HBs, but we will show shortly that neglecting such interactions does not affect overall trends since this contribution to adsorption is similar for all FGs except for a few in our data set.

We first validate the correlation of the CHBS with overall ΔE_{ads} on minimal models (MMs) representative of the Fc^+ FGs (e.g., an NH_3 molecule model for the amine (**1**) FG) that also span a wide HB-donating ability range and compare to correlations of the CHBS with the anion/FG−Fc^+ complex (Figure 8 and Supporting Information Table S9). For formate (Figure 8a), the MMs correlate extremely well (R^2 = 0.99) to the CHBS with the exception of the excluded phosphine outlier that forms no HBs due to the low electronegativity of phosphorus. Formate/FG−Fc^+ complex ΔE_{ads} values are well correlated with the CHBS (R^2 = 0.89), after excluding three outliers. Overall, the increased scatter in the full complex compared to the minimal models is primarily due to the variable penalty for distortion in the full complex. For the formate/FG−Fc^+ complex outliers (−PPh_2 (**6**), −NCS (**41**), and −CCl_3 (**34**)), strong non-HB dipole−dipole interactions

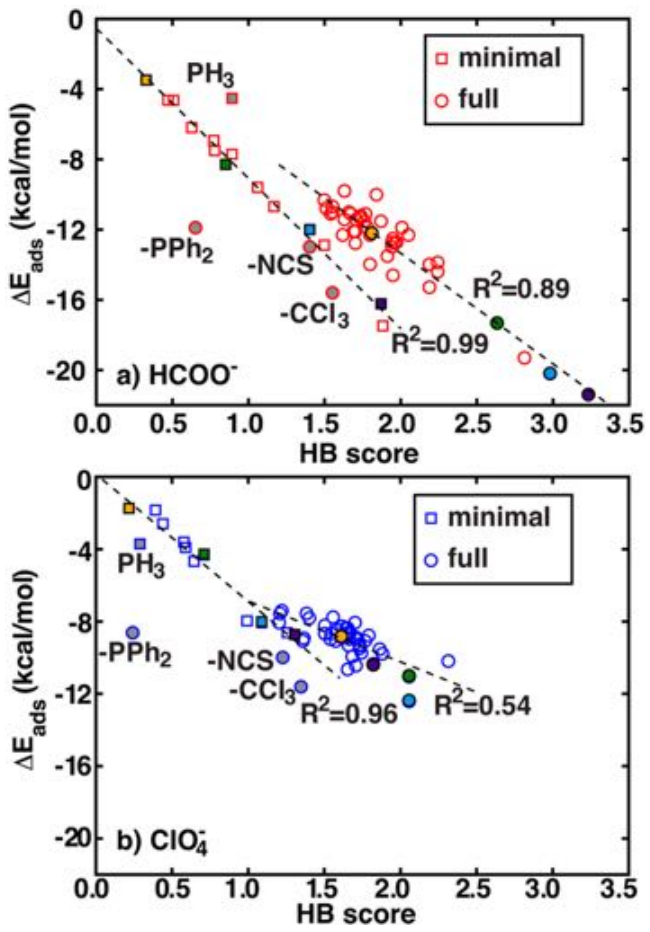

Figure 8. (a) Formate (red) and (b) perchlorate (blue) ΔE_{ads} (kcal/mol) versus HB score for (i) minimal models (squares) and (ii) FG−Fc^+ structures (circles). The PPh_2 (**6**), NCS (**41**), and CCl_3 (**34**) outliers, indicated as gray-filled circles, are excluded from the black dashed linear best fits. Selected symbols are color-coded (orange, green, blue, and purple) to aid comparison of the minimal models to the FG−Fc^+ structures.

that are not captured in the CHBS (e.g., a C···O interaction between −NCS and formate) likely increase ΔE_{ads} without increasing the CHBS, though the P···O interaction in FG **6** appears to be sensitive to basis set size (Supporting Information Table S1 and Figure S1). We note that in all cases the CHBS improves substantially over averaging HB distances alone (Supporting Information Figure S5).

We selected individual minimal models (CH_4 in orange, NH_3 in green, amide in light blue, CH_3OH in purple) that are analogous to FG−Fc^+ structures (methyl (**36**), amine (**1**), amide (**44**), alkanolamine (**43**), same fill) and span the ΔE_{ads} range. Ranking and placement are consistent for these four groups when comparing ΔE^f_{ads} to MMs or complexes. Trends in formate adsorption to MMs and full FG−Fc^+ complexes are aligned with close slopes of −8.6 kcal/mol (MMs) and −6.3 kcal/mol (complexes) and a slight upward shift for the full FG−Fc^+ complexes, indicating the additivity approximation works well. We attribute the shift and shallower slope of FG−Fc^+ to distortion energy required to accommodate HBs absent from the MMs.

For perchlorate, the relationship between the CHBS and ΔE_{ads} for MMs is quite good (R^2 = 0.96), but the correlation for the full FG−Fc^+ complexes (R^2 = 0.54) is substantially

DOI: 10.1021/acs.chemmater.6b02378
Chem. Mater. 2016, 28, 6207−6218

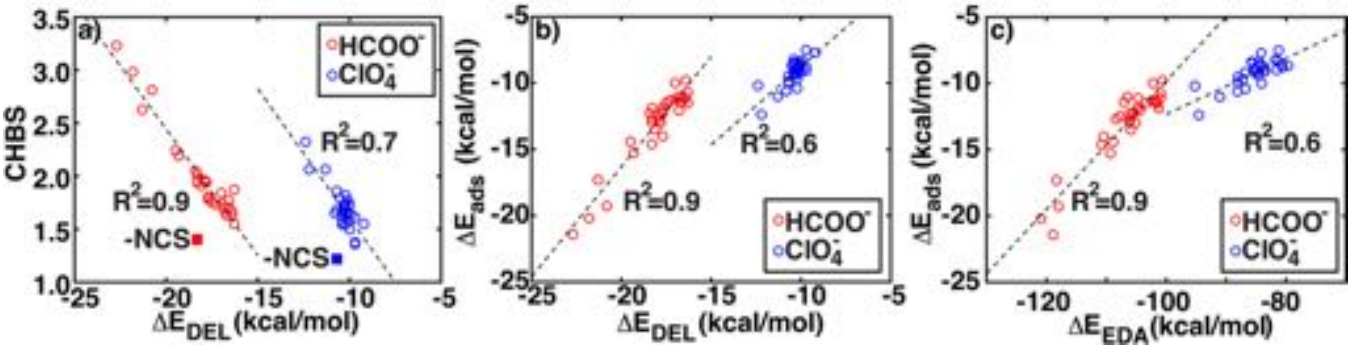

Figure 9. EDA correlations for formate and perchlorate. From left to right: (a) CHBS vs EDA DEL energy, (b) solvated ΔE_{ads} vs EDA ΔE_{DEL}, and (c) solvated ΔE_{ads} vs EDA gas phase rigid adsorption energy, ΔE_{EDA}. The black dashed lines indicate linear best-fits, and the NCS (**41**) CHBS outlier, indicated as a filled square in panel a is excluded.

lower (Figure 8b) than the one observed for formate (Figure 8a). The weaker complex correlation is attributable to the smaller CHBS range spanned by perchlorate without any decrease in the contribution of distortion energy variations to the residuals. The root-mean-square error of prediction is similar at 0.9 kcal/mol for formate and 0.7 kcal/mol for perchlorate. The slopes of −7.0 kcal/mol for the MMs and −3.4 kcal/mol for the complexes are both lower than was observed for formate and more distinct. The difference between the MMs and complexes with perchlorate can be attributed to the geometric constraints described earlier and wider confidence intervals in the complexes. The reasonable fits across MMs and complexes confirm that the anion−Fc^+ intermolecular interactions are largely composed of additive HB donor−acceptor interactions for both perchlorate and formate, with weaker overall HBs for perchlorate. Weaker HBs in perchlorate complexes are confirmed by two other observations: (i) ordering and placement of MMs and corresponding FG−Fc^+ complexes no longer agree for perchlorate, which we would expect if the HBs individually contribute less to the overall ΔE_{ads}; (ii) both water and methanol have weaker ΔE^{p}_{ads} than ΔE^{f}_{ads} despite the larger dispersion contribution for perchlorate.

We performed energy decomposition analysis (EDA) on the solvent-optimized geometries to further investigate the charge transfer (DEL, in EDA nomenclature), electrostatic (FRZ), and polarization (POL) contributions to overall adsorption energies (see Supporting Information Table S10). In particular, charge transfer from HB acceptor to HB donor, which can be readily probed with EDA, is generally accepted as a key characteristic of the HB,[56,99] even though the exact quantum mechanical nature of the HB is still under debate.[55,56,102−104] To identify whether variations in dispersion energy played a significant role in FG selectivity, we compared the dispersion contribution to binding but found minimal variation and correlation between FGs, suggesting directional hydrogen bonding interactions dominate over any dispersion contribution to selectivity (Supporting Information Tables S11 and S12 and Figure S6). Solvent ΔE_{ads} correlates well with the calculated with rigid-binding-approximation EDA adsorption energy (ΔE_{EDA}) in the gas phase (R^2 = 0.9 for formate, 0.6 for perchlorate shown in Figure 9c), suggesting the transferability of EDA trends across a range of dielectric environments. In select cases, charge transfer was overestimated in the gas phase, leading to inaccurate EDA and those were omitted (Supporting Information Table S2). Weaker correlations are again observed for perchlorate due to a narrower energy range without a decrease in the residuals.

The DEL contribution (ΔE_{DEL}) to ΔE_{EDA}, which measures stabilization due to charge transfer, correlates well with both the CHBS (eqs 6 and 7) and solvent ΔE_{ads} for both anions (Figure 9a,b), excluding only one previously discussed −NCS (**41**) outlier. This correlation is significantly stronger than for the electrostatic or polarization components (FRZ and POL correlations are plotted in Supporting Information Figure S7). Notably, the ΔE_{DEL} contribution is significantly lower for perchlorate than formate across all FGs, confirming the general weakness of perchlorate HBs compared to formate HBs through lower charge transfer.

We then considered other factors that might affect relative perchlorate/formate ΔE_{ads} with FG−Fc^+ complexes including through-space electrostatic interactions and variations in the electronic structure of the Fc^+ core. Through-space electrostatic interactions were approximated by the inverse Fe to anion center of mass (ACOM) distance, and individual FG−Fc^+ electronic properties were represented by the Fe NBO partial charge and Fe delocalization index to neighboring atoms. Despite demonstrated utility[105,106] of these quantities as descriptors for binding energies, none of the three descriptors demonstrated improved correlation to ΔE_{ads} compared to the CHBS or EDA DEL energy for either anion (Supporting Information Table S13). Although through-space electrostatic interactions are likely significant over larger ranges of Fe-ACOM distances,[106] individual directional HBs quantified in the CHBS mediate electrostatic attraction at close distances. The partial charge and delocalization index of Fe provides an indirect measure of the FG electron donating/withdrawing ability, but this effect is outweighed by direct HBs formed between the anion and FG when they are placed in close proximity. Moderate correlations with core electronic properties are only observed for weaker, indirect adsorption cases (Supporting Information Figure S3). Instead, we attribute Fc^+ and FG−Fc^+ selectivity for formate to partially covalent C−H···O bonds[99] in anion/FG−Fc^+ complexes, as evidenced by QTAIM BCPs and the DEL correlation to CHBS, that are stronger, shorter, and more directional for formate than perchlorate.

3d. Adsorption on Reduced Ferrocene. To maximize selectivity, we have initially identified strong HB-donating groups (e.g., amides) that maximize formate adsorption and selectivity, consistent with experimental studies on selective anion recognition by amide-substituted Fc^+ moieties.[24,42] In

DOI: 10.1021/acs.chemmater.6b02378
Chem. Mater. 2016, 28, 6207−6218

contrast to those earlier studies, rapid and selective electrochemical separation requires that FG−Fc^+ selectivity for formate is increased while rapid desorption at the reduced Fc polymer electrode is maintained. Thus, we computed formate ΔE_{ads} with neutral Fc for all FGs and found them to correlate well (R^2 = 0.9) with oxidized formate−Fc^+ ΔE_{ads} (Figure 10).

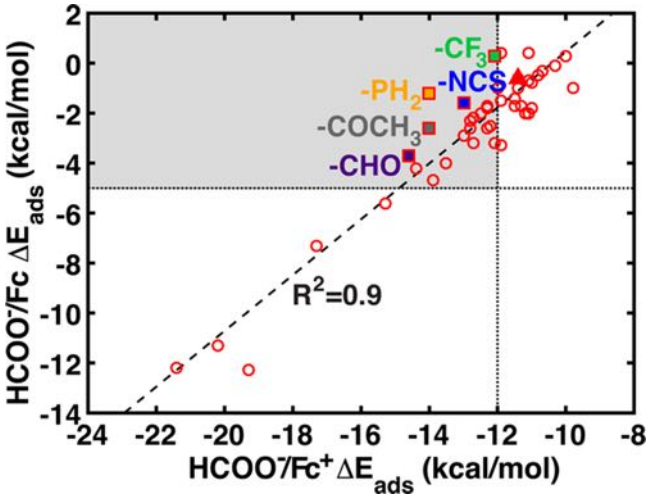

Figure 10. Formate−Fc^+ complex adsorption energy versus formate−Fc adsorption energy with black dashed best-fit line (R^2 = 0.9). The shaded quadrant and black dotted lines indicate the constrained design space. The unfunctionalized case is shown as a filled triangle and selected functionalizations that fall within the design space are labeled with text in the same color as the filled squares.

The 1.1 (kcal/mol $\Delta E_{ads}^{Fc\text{-}f}$)/(kcal/mol $\Delta E_{ads}^{Fc^+\text{-}f}$) slope across the ΔE_{ads} range suggests that FG-derived increase in formate adsorption and selectivity at Fc^+ will also increase adsorption to reduced Fc, discouraging the use of the strongest HB-donating groups favored in supramolecular chemistry. Indeed, we can divide the relationship between neutral and oxidized Fc^+ adsorption ($\frac{\Delta E_{ads}^{Fc\text{-}f}}{\Delta E_{ads}^{Fc^+\text{-}f}}$ = 1.1, Figure 10) by formate−perchlorate selectivity at Fc^+ ($\frac{\Delta E_{ads}^{f\text{-}p}}{\Delta E_{ads}^{Fc^+\text{-}f}}$ = 0.66, eq 5 and Figure 5) to determine that a 1.0 kcal/mol enhancement of $\Delta E_{ads}^{f\text{-}p}$ simultaneously increases formate−Fc adsorption by 1.7 kcal/mol, suggesting a delicate balance is required in tuning selectivity.

Alternative mechanisms for promoting formate desorption in strongly bonded complexes could be increasing the temperature or decreasing the pH. The former strategy may be challenging to implement because electrostatic interactions are concomitantly strengthened by the decrease in dielectric constant with temperature for most solvents. In the latter case, pH adjustments would be somewhat limited by the extent of FG−Fc hydrogen bonding with formic acid that is still quite strong (Supporting Information Table S14). Thus, for reversible adsorption at Fc^+ with unchanged solution conditions upon reduction, our design space is constrained (shaded region in Figure 10) both by (i) increasing $\Delta E_{ads}^{f\text{-}p}$ over Fc^+ ($\Delta E_{ads}^{Fc^+\text{-}f}$ = −12 kcal/mol from Figure 5 correlation, vertical dotted line in Figure 10) and (ii) a minimum formate desorption rate. We define the minimum desorption rate as 0.1% of that for Fc at 298 K, which is a 4 kcal/mol increase in $\Delta E_{ads}^{Fc\text{-}f}$ over Fc (horizontal dotted line in Figure 10).

Within the constrained design space quadrant, phosphine (−PH_2 (**5**), orange symbol in Figure 10), isothiocyanate (−NCS (**41**), blue symbol), and trifluoromethyl (−CF_3 (**35**), green symbol), are promising for their unusually weak $\Delta E_{ads}^{Fc\text{-}f}$ values. The disproportionately weak $\Delta E_{ads}^{Fc\text{-}f}$ may be explained by non-HB interactions that are much weaker with reduced Fc compared to HBs. However, these groups are also less ideal from an experimental perspective due to potential reactivity: −PH_2 is easily oxidized and −NCS and −CF_3 are hydrolyzed.[107] Our constrained design space also includes the stable aldehyde (−CHO (**14**), purple in Figure 10), methyl ketone (−$COCH_3$ (**18**), gray symbol), and isopropyl sulfide (**28**) FGs. Although most of these FGs would be suitable candidates for experimental electrochemical separations, the aldehyde (**14**) and isopropyl sulfide (**28**) FGs display the largest $\Delta E_{ads}^{f\text{-}p}$ selectivities.

3e. Identifying and Abstracting Ideal HB Interactions. In particular, the aldehyde (**14**) FG binds less strongly to Fc, is readily available and widely used, typically as a synthetic intermediate to other substituted ferrocenes.[108] The atom-efficient aldehyde functionalization (**14**) illustrates the design principles determined in this study, and its planarity and size minimize variability from conformational isomerism. Geometrically, the placement of the hydrogen atom in (**14**) away from the Cp^- rings alleviates unfunctionalized Fc^+−formate geometric constraints through formation of an additional short HB with angle close to 140°. Electronically, the aldehyde hydrogen is an intermediate HB donor due the polarity of the C═O bond, also evident from the low C−H···O distance of 2.17 Å and the associated HBS. Selectivity is enhanced because the perchlorate HB strength increases less and perchlorate is unable to form greater numbers of HBs. Additionally, anion adsorption on the O-containing side of the aldehyde FG is 4 kcal/mol weaker due to the repulsive carbonyl oxygen atom and absence of an HB donor, which could be used in the future for spatial control of anion adsorption.

Using these suggested FGs, we introduce the concept of a materiaphore, which is an extension of the pharmacophore concept widely employed in therapeutic drug discovery,[109] for iterative computational materials discovery. The materiaphore is an abstraction of the key design principles unearthed thus far that enables identifying new materials with the desired features for selective, reversible carboxylate adsorption in electrochemical separations. Through this abstraction, we (i) identify a series of geometric and electronic descriptors for rapid screening of atomic and geometric properties often without the full computational cost of DFT calculations and (ii) no longer restrict the material to a Fc^+/Fc polymer electrode. A materiaphore encapsulating the design principles needed for selective, electrochemical adsorption of formate is illustrated in Figure 11. In our materiaphore, we leverage the pharmacophore concepts of the HB donor representation (dotted magenta spheres) with annotated distances. We also emphasize a targeted moderate polarity for any HB donors and introduce the mandate of a proximal redox active center through the red sphere representation. Guided by the materiaphore representation, we then screened two-FG combinations and identified that adding a vinyl group (**37**) to the bottom Cp^- ring alongside the previously identified aldehyde (**14**) produced an increase of $\Delta E_{ads}^{f\text{-}p}$ to −6.6 kcal/mol or over 2 kcal/mol above the single (**14**) FG. Importantly, this added FG preserved a suitable formate−FG−Fc^+/FG−Fc adsorption energy, and the

DOI: 10.1021/acs.chemmater.6b02378
Chem. Mater. 2016, 28, 6207−6218

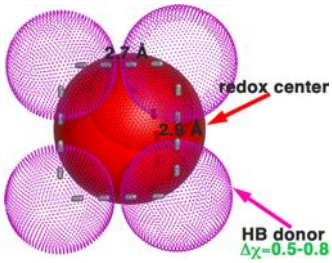

Figure 11. Illustration of the ideal materiaphore for selective, electrochemical carboxylate adsorption. Hydrogen bond donors are indicated as magenta dotted spheres, a redox-active center by a red sphere, and suggested relative polarity and distances are annotated.

geometry closely resembled the materiaphore target geometry (see Supporting Information for coordinates).

4. CONCLUSIONS

Using a first-principles computational screening approach, we have investigated and rationalized the effect of Fc/Fc^+ FGs on the selectivity and reversibility of formate−Fc^+ adsorption with respect to perchlorate. The wide design space of 44 FGs enabled us to find (i) a clear positive correlation between formate adsorption strength and formate−perchlorate selectivity and (ii) 14 FG−Fc^+s with higher selectivity than standard Fc^+. Across this design space, we developed the CHBS and analyzed stabilization due to charge transfer with EDA to identify that formate selectivity at Fc^+ in aqueous conditions could be strengthened either (i) electronically via introduction of HB donors stronger than the Cp^- hydrogen, or (ii) geometrically via placement of additional HB donors of any strength closer to formate than the original Cp^- hydrogen. Both approaches increase formate selectivity because perchlorate forms individually weaker HBs with HB donors than formate, indicated both by geometric effects (distance and angle of HBs) and electronic effects with lower charge transfer contribution to adsorption, suggesting more covalent character in formate C−H···O bonds. Formate adsorption was weakened when the FG disrupted already favorable formate−Cp^- interactions, increasing perchlorate preference because its larger size and number of HB acceptors support favorable adsorption with more varied FGs.

For reversible applications, the Fc^+ electrode material should release the selectively bound ions when reduced to Fc. We identified that strong HB donor FGs that strengthened Fc^+-formate adsorption simultaneously strengthened interactions of the anions with neutral Fc even more so. Thus, widely used motifs in supramolecular chemistry were found to bind too strongly in the reduced state for reasonable desorption rates. Narrowing our design space accordingly, we suggested instead intermediate HB aldehyde and isopropylsulfide donors that are experimentally stable and improve formate selectivity at Fc^+ with only a modest increase in adsorption to Fc.

Finally, we introduced the materiaphore abstraction via screening of doubly functionalized Fc^+s and identified that (**14**),(**37**)−Fc^+ not only maintained but increased formate selectivity over the single FG cases. We expect the approach presented here to design hydrogen bonds for selective interactions in realistic, aqueous conditions has broad applicability to molecular recognition, sensing, separations, and catalysis beyond the Fc/Fc^+ system alone. More immediate application of our findings will be to optimize selectivity of FG−Fc^+ for other desirable anions such as sulfonates and to identify strategies for enhancing the recently demonstrated[110] electrocatalytic activity of the Fc/Fc^+ electrode. Further work is under way in our group to automate and broadly apply this chemical discovery approach.

■ ASSOCIATED CONTENT

Supporting Information

The Supporting Information is available free of charge on the ACS Publications website at DOI: 10.1021/acs.chemmater.6b02378.

Structures of binding modes (ZIP).

Additional computational details; larger basis set results; comparison of B3LYP and ωPBEh results; solvation/complexation thermodynamic cycle; custom core coordinates; electronic descriptor correlations for indirect adsorption data set; evaluation of entropy/ZPVE contributions; functional groups excluded from final list; estimated basicities of ionizable functional groups; classification of functional groups by largest electronegativity difference; geometries of all hydrogen bonds; minimal model adsorption energies; correlations based on average hydrogen bond distance; adsorption energies, CHBS and EDA component energies; evaluation of dispersion contributions; frozen-density and polarization contribution correlations; least-squares regressions of alternate geometric and electronic descriptors (PDF).

Structures of optimized functionalized ferrocene (ZIP).

■ AUTHOR INFORMATION

Corresponding Author

*H. J. Kulik. Email: hjkulik@mit.edu. Phone: 617-253-4584.

Notes

The authors declare no competing financial interest.

■ ACKNOWLEDGMENTS

This work was supported by a Reed grant from the MIT Research Support Corporation and an MIT Energy Initiative Seed Grant. The authors acknowledge partial support by the National Science Foundation under grant number ECCS-1449291. H.J.K. holds a Career Award at the Scientific Interface from the Burroughs Wellcome Fund. This work was carried out in part using computational resources from the Extreme Science and Engineering Discovery Environment (XSEDE), which is supported by National Science Foundation grant number ACI-1053575. The authors thank Jeong-Yun Kim and Adam H. Steeves for providing a critical reading of the paper.

■ REFERENCES

(1) Koros, W. J.; Lively, R. P. Water and Beyond: Expanding the Spectrum of Large-Scale Energy Efficient Separation Processes. *AIChE J.* **2012**, *58*, 2624−2633.

(2) Wang, S.; Peng, Y. Natural Zeolites as Effective Adsorbents in Water and Wastewater Treatment. *Chem. Eng. J.* **2010**, *156*, 11−24.

(3) Kim, J.; Tsouris, C.; Mayes, R. T.; Oyola, Y.; Saito, T.; Janke, C. J.; Dai, S.; Schneider, E.; Sachde, D. Recovery of Uranium from Seawater: A Review of Current Status and Future Research Needs. *Sep. Sci. Technol.* **2013**, *48*, 367−387.

(4) Grondal, C.; Jeanty, M.; Enders, D. Organocatalytic Cascade Reactions as a New Tool in Total Synthesis. *Nat. Chem.* **2010**, *2*, 167−178.

(5) Henley, E. J.; Seader, J. D.; Roper, D. K. *Separation Process Principles*; Wiley: New York, 2011.

DOI: 10.1021/acs.chemmater.6b02378
Chem. Mater. 2016, 28, 6207−6218

(6) Kumar, B.; Llorente, M.; Froehlich, J.; Dang, T.; Sathrum, A.; Kubiak, C. P. Photochemical and Photoelectrochemical Reduction of CO_2. *Annu. Rev. Phys. Chem.* **2012**, *63*, 541−569.
(7) Schuchmann, K.; Müller, V. Direct and Reversible Hydrogenation of CO_2 to Formate by a Bacterial Carbon Dioxide Reductase. *Science* **2013**, *342*, 1382−1385.
(8) Whipple, D. T.; Kenis, P. J. A. Prospects of CO_2 Utilization Via Direct Heterogeneous Electrochemical Reduction. *J. Phys. Chem. Lett.* **2010**, *1*, 3451−3458.
(9) Enthaler, S.; von Langermann, J.; Schmidt, T. Carbon Dioxide and Formic Acid—the Couple for Environmental-Friendly Hydrogen Storage? *Energy Environ. Sci.* **2010**, *3*, 1207−1217.
(10) Hull, J. F.; Himeda, Y.; Wang, W.-H.; Hashiguchi, B.; Periana, R.; Szalda, D. J.; Muckerman, J. T.; Fujita, E. Reversible Hydrogen Storage Using CO_2 and a Proton-Switchable Iridium Catalyst in Aqueous Media under Mild Temperatures and Pressures. *Nat. Chem.* **2012**, *4*, 383−388.
(11) Sholl, D. S.; Lively, R. P. Seven Chemical Separations to Change the World. *Nature* **2016**, *532*, 435−437.
(12) Beer, P. D.; Gale, P. A. Anion Recognition and Sensing: The State of the Art and Future Perspectives. *Angew. Chem., Int. Ed.* **2001**, *40*, 486−516.
(13) Wang, R. Y.; Shyam, B.; Stone, K. H.; Weker, J. N.; Pasta, M.; Lee, H. W.; Toney, M. F.; Cui, Y. Reversible Multivalent (Monovalent, Divalent, Trivalent) Ion Insertion in Open Framework Materials. *Adv. Energy Mater.* **2015**, *5*, 1401869.
(14) Dash, A.; Chakravarty, R. Electrochemical Separation: Promises, Opportunities, and Challenges to Develop Next-Generation Radionuclide Generators to Meet Clinical Demands. *Ind. Eng. Chem. Res.* **2014**, *53*, 3766−3777.
(15) Suss, M. E.; Porada, S.; Sun, X.; Biesheuvel, P. M.; Yoon, J.; Presser, V. Water Desalination Via Capacitive Deionization: What Is It and What Can We Expect from It? *Energy Environ. Sci.* **2015**, *8*, 2296−2319.
(16) Su, X.; Kulik, H. J.; Jamison, T. F.; Hatton, T. A. Anion-Selective Redox Electrodes: Electrochemically Mediated Separation with Heterogeneous Organometallic Interfaces. *Adv. Funct. Mater.* **2016**, *26*, 3394−3404.
(17) Ding, Y.; Zhao, Y.; Yu, G. A Membrane-Free Ferrocene-Based High-Rate Semiliquid Battery. *Nano Lett.* **2015**, *15*, 4108−4113.
(18) Whittell, G. R.; Manners, I. Metallopolymers: New Multifunctional Materials. *Adv. Mater.* **2007**, *19*, 3439−3468.
(19) Mao, X.; Simeon, F.; Rutledge, G. C.; Hatton, T. A. Electrospun Carbon Nanofiber Webs with Controlled Density of States for Sensor Applications. *Adv. Mater.* **2013**, *25*, 1309−1314.
(20) Yang, Y.; Yu, L. Theoretical Investigations of Ferrocene/Ferrocenium Solvation in Imidazolium-Based Room-Temperature Ionic Liquids. *Phys. Chem. Chem. Phys.* **2013**, *15*, 2669−2683.
(21) Stone, D. L.; Smith, D. K. Anion Binding at the Core of Branched Ferrocene Derivatives. *Polyhedron* **2003**, *22*, 763−768.
(22) Coles, S. J.; Denuault, G.; Gale, P. A.; Horton, P. N.; Hursthouse, M. B.; Light, M. E.; Warriner, C. N. Mono- and Bis-Ferrocene 2,5-Diamidopyrrole Clefts: Solid-State Assembly, Anion Binding and Electrochemical Properties. *Polyhedron* **2003**, *22*, 699−709.
(23) Zhuo, J.-B.; Zhang, C.-Y.; Lin, C.-X.; Bai, S.; Xie, L.-L.; Yuan, Y.-F. Acyclic Ferrocene-Based Imidazolium Salts as Multi-Site Anion Receptors. *J. Organomet. Chem.* **2014**, *763*−*764*, 34−43.
(24) Beer, P. D. Transition-Metal Receptor Systems for the Selective Recognition and Sensing of Anionic Guest Species. *Acc. Chem. Res.* **1998**, *31*, 71−80.
(25) Zhang, Z.; Schreiner, P. R. (Thio) Urea Organocatalysis—What Can Be Learnt from Anion Recognition? *Chem. Soc. Rev.* **2009**, *38*, 1187−1198.
(26) Amendola, V.; Fabbrizzi, L.; Mosca, L. Anion Recognition by Hydrogen Bonding: Urea-Based Receptors. *Chem. Soc. Rev.* **2010**, *39*, 3889−3915.
(27) Hua, Y.; Flood, A. H. Click Chemistry Generates Privileged CH Hydrogen-Bonding Triazoles: The Latest Addition to Anion Supramolecular Chemistry. *Chem. Soc. Rev.* **2010**, *39*, 1262−1271.
(28) Schreiner, P. R. Metal-Free Organocatalysis through Explicit Hydrogen Bonding Interactions. *Chem. Soc. Rev.* **2003**, *32*, 289−296.
(29) Taylor, M. S.; Jacobsen, E. N. Asymmetric Catalysis by Chiral Hydrogen-Bond Donors. *Angew. Chem., Int. Ed.* **2006**, *45*, 1520−1543.
(30) Malerich, J. P.; Hagihara, K.; Rawal, V. H. Chiral Squaramide Derivatives Are Excellent Hydrogen Bond Donor Catalysts. *J. Am. Chem. Soc.* **2008**, *130*, 14416−14417.
(31) Roberts, J. M.; Fini, B. M.; Sarjeant, A. A.; Farha, O. K.; Hupp, J. T.; Scheidt, K. A. Urea Metal−Organic Frameworks as Effective and Size-Selective Hydrogen-Bond Catalysts. *J. Am. Chem. Soc.* **2012**, *134*, 3334−3337.
(32) Cleland, W. W.; Kreevoy, M. M. Low-Barrier Hydrogen Bonds and Enzymic Catalysis. *Science* **1994**, *264*, 1887−1890.
(33) Lipinski, C. A.; Lombardo, F.; Dominy, B. W.; Feeney, P. J. Experimental and Computational Approaches to Estimate Solubility and Permeability in Drug Discovery and Development Settings. *Adv. Drug Delivery Rev.* **2012**, *64*, 4−17.
(34) Craik, D. J.; Fairlie, D. P.; Liras, S.; Price, D. The Future of Peptide-Based Drugs. *Chem. Biol. Drug Des.* **2013**, *81*, 136−147.
(35) Congreve, M.; Andrews, S. P.; Doré, A. S.; Hollenstein, K.; Hurrell, E.; Langmead, C. J.; Mason, J. S.; Ng, I. W.; Tehan, B.; Zhukov, A.; Weir, M.; Marshall, F. H. Discovery of 1, 2, 4-Triazine Derivatives as Adenosine A2a Antagonists Using Structure Based Drug Design. *J. Med. Chem.* **2012**, *55*, 1898−1903.
(36) Vulpetti, A.; Dalvit, C. Fluorine Local Environment: From Screening to Drug Design. *Drug Discovery Today* **2012**, *17*, 890−897.
(37) Roesky, H. W.; Andruh, M. The Interplay of Coordinative, Hydrogen Bonding and $\pi-\pi$ Stacking Interactions in Sustaining Supramolecular Solid-State Architectures.: A Study Case of Bis (4-Pyridyl)-and Bis (4-Pyridyl-N-Oxide) Tectons. *Coord. Chem. Rev.* **2003**, *236*, 91−119.
(38) Cordier, P.; Tournilhac, F.; Soulié-Ziakovic, C.; Leibler, L. Self-Healing and Thermoreversible Rubber from Supramolecular Assembly. *Nature* **2008**, *451*, 977−980.
(39) Yan, X.; Li, S.; Pollock, J. B.; Cook, T. R.; Chen, J.; Zhang, Y.; Ji, X.; Yu, Y.; Huang, F.; Stang, P. J. Supramolecular Polymers with Tunable Topologies Via Hierarchical Coordination-Driven Self-Assembly and Hydrogen Bonding Interfaces. *Proc. Natl. Acad. Sci. U. S. A.* **2013**, *110*, 15585−15590.
(40) Yoon, J.; Kim, S. K.; Singh, N. J.; Kim, K. S. Imidazolium Receptors for the Recognition of Anions. *Chem. Soc. Rev.* **2006**, *35*, 355−360.
(41) Chen, B.; Wang, L.; Zapata, F.; Qian, G.; Lobkovsky, E. B. A Luminescent Microporous Metal− Organic Framework for the Recognition and Sensing of Anions. *J. Am. Chem. Soc.* **2008**, *130*, 6718−6719.
(42) Beer, P. D.; Drew, M. G.; Hesek, D.; Nam, K. C. A New Carboxylate Anion Selective Cobaltocenium Calix[4]Arene Receptor. *Chem. Commun.* **1997**, 107−108.
(43) Miyaji, H.; Collinson, S. R.; Prokeš, I.; Tucker, J. H. A Ditopic Ferrocene Receptor for Anions and Cations That Functions as a Chromogenic Molecular Switch. *Chem. Commun.* **2003**, 64−65.
(44) Coriani, S.; Haaland, A.; Helgaker, T.; Jørgensen, P. The Equilibrium Structure of Ferrocene. *ChemPhysChem* **2006**, *7*, 245−249.
(45) Zhang, W.-W.; Yu, Y.-G.; Lu, Z.-D.; Mao, W.-L.; Li, Y.-Z.; Meng, Q.-J. Ferrocene-Phenothiazine Conjugated Molecules: Synthesis, Structural Characterization, Electronic Properties, and DFT-TDDFT Computational Study. *Organometallics* **2007**, *26*, 865−873.
(46) Muller, T. J.; Conradie, J.; Erasmus, E. A Spectroscopic, Electrochemical and DFT Study of Para-Substituted Ferrocene-Containing Chalcone Derivatives: Structure of Fccochch(P-Tbuc6h4). *Polyhedron* **2012**, *33*, 257−266.
(47) Beer, P. D.; Graydon, A. R.; Johnson, A. O.; Smith, D. K. Neutral Ferrocenoyl Receptors for the Selective Recognition and Sensing of Anionic Guests. *Inorg. Chem.* **1997**, *36*, 2112−2118.

DOI: 10.1021/acs.chemmater.6b02378
Chem. Mater. 2016, 28, 6207−6218

(48) Beer, P. D.; Gale, P. A.; Chen, G. Z. Mechanisms of Electrochemical Recognition of Cations, Anions and Neutral Guest Species by Redox-Active Receptor Molecules. *Coord. Chem. Rev.* **1999**, *185*, 3−36.
(49) Ramabhadran, R. O.; Hua, Y.; Flood, A. H.; Raghavachari, K. C Vs N: Which End of the Cyanide Anion Is a Better Hydrogen Bond Acceptor? *J. Phys. Chem. A* **2014**, *118*, 7418−7423.
(50) Hunter, C. A. Quantifying Intermolecular Interactions: Guidelines for the Molecular Recognition Toolbox. *Angew. Chem., Int. Ed.* **2004**, *43*, 5310−5324.
(51) Abraham, M. H.; Platts, J. A. Hydrogen Bond Structural Group Constants. *J. Org. Chem.* **2001**, *66*, 3484−3491.
(52) Abraham, M. H.; Acree, W. E.; Earp, C. E.; Vladimirova, A.; Whaley, W. L. Studies on the Hydrogen Bond Acidity, and Other Descriptors and Properties for Hydroxyflavones and Hydroxyisoflavones. *J. Mol. Liq.* **2015**, *208*, 363−372.
(53) Gilli, G.; Gilli, P. *The Nature of the Hydrogen Bond: Outline of a Comprehensive Hydrogen Bond Theory*; OUP Oxford, 2009.
(54) Weinhold, F.; Klein, R. A. What Is a Hydrogen Bond? Mutually Consistent Theoretical and Experimental Criteria for Characterizing H-Bonding Interactions. *Mol. Phys.* **2012**, *110*, 565−579.
(55) Weinhold, F.; Klein, R. A. Anti-Electrostatic Hydrogen Bonds. *Angew. Chem., Int. Ed.* **2014**, *53*, 11214−11217.
(56) Arunan, E.; Desiraju, G. R.; Klein, R. A.; Sadlej, J.; Scheiner, S.; Alkorta, I.; Clary, D. C.; Crabtree, R. H.; Dannenberg, J. J.; Hobza, P.; et al. Definition of the Hydrogen Bond (Iupac Recommendations 2011). *Pure Appl. Chem.* **2011**, *83*, 1637−1641.
(57) Desiraju, G. R. The Ch··· O Hydrogen Bond: Structural Implications and Supramolecular Design. *Acc. Chem. Res.* **1996**, *29*, 441−449.
(58) Steiner, T.; Desiraju, G. R. Distinction between the Weak Hydrogen Bond and the Van Der Waals Interaction. *Chem. Commun.* **1998**, 891−892.
(59) Desiraju, G. R.; Steiner, T. *The Weak Hydrogen Bond: In Structural Chemistry and Biology*; Oxford University Press on Demand, 2001; Vol. *9*.
(60) Weiss, M. S.; Brandl, M.; Sühnel, J.; Pal, D.; Hilgenfeld, R. More Hydrogen Bonds for the (Structural) Biologist. *Trends Biochem. Sci.* **2001**, *26*, 521−523.
(61) Donahue, J. Selected Topics in Hydrogen Bonding. In *Structural Chemistry and Molecular Biology*; Rich, A.; Davidson, N. R.; Pauling, L., Eds.; **1968**; pp 443−465.
(62) Cotton, F. A.; Daniels, L. M.; Jordan, G. T., IV; Murillo, C. A. The Crystal Packing of Bis (2, 2′-Dipyridylamido) Cobalt (Ii), Co (Dpa) 2, Is Stabilized by C−H··· N Bonds: Are There Any Real Precedents? *Chem. Commun.* **1997**, 1673−1674.
(63) Taylor, R.; Kennard, O. Crystallographic Evidence for the Existence of Ch···O, Ch··· N and Ch··· Cl Hydrogen Bonds. *J. Am. Chem. Soc.* **1982**, *104*, 5063−5070.
(64) Gu, Y.; Kar, T.; Scheiner, S. Fundamental Properties of the Ch··· O Interaction: Is It a True Hydrogen Bond? *J. Am. Chem. Soc.* **1999**, *121*, 9411−9422.
(65) Vargas, R.; Garza, J.; Dixon, D. A.; Hay, B. P. How Strong Is the Cα-H··· Oc Hydrogen Bond? *J. Am. Chem. Soc.* **2000**, *122*, 4750−4755.
(66) Greeley, J.; Jaramillo, T. F.; Bonde, J.; Chorkendorff, I.; Nørskov, J. K. Computational High-Throughput Screening of Electrocatalytic Materials for Hydrogen Evolution. *Nat. Mater.* **2006**, *5*, 909−913.
(67) Nørskov, J. K.; Bligaard, T.; Rossmeisl, J.; Christensen, C. H. Towards the Computational Design of Solid Catalysts. *Nat. Chem.* **2009**, *1*, 37−46.
(68) Jensen, P. B.; Bialy, A.; Blanchard, D.; Lysgaard, S.; Reumert, A. K.; Quaade, U. J.; Vegge, T. Accelerated DFT-Based Design of Materials for Ammonia Storage. *Chem. Mater.* **2015**, *27*, 4552−4561.
(69) Hautier, G.; Fischer, C. C.; Jain, A.; Mueller, T.; Ceder, G. Finding Nature's Missing Ternary Oxide Compounds Using Machine Learning and Density Functional Theory. *Chem. Mater.* **2010**, *22*, 3762−3767.
(70) Jain, A.; Hautier, G.; Moore, C. J.; Ong, S. P.; Fischer, C. C.; Mueller, T.; Persson, K. A.; Ceder, G. A High-Throughput Infrastructure for Density Functional Theory Calculations. *Comput. Mater. Sci.* **2011**, *50*, 2295−2310.
(71) Hautier, G.; Miglio, A.; Ceder, G.; Rignanese, G.-M.; Gonze, X. Identification and Design Principles of Low Hole Effective Mass P-Type Transparent Conducting Oxides. *Nat. Commun.* **2013**, *4*, 2292.
(72) Grimme, S.; Antony, J.; Ehrlich, S.; Krieg, H. A Consistent and Accurate Ab Initio Parametrization of Density Functional Dispersion Correction (DFT-D) for the 94 Elements H-Pu. *J. Chem. Phys.* **2010**, *132*, 154104.
(73) Dion, M.; Rydberg, H.; Schröder, E.; Langreth, D. C.; Lundqvist, B. I. Van Der Waals Density Functional for General Geometries. *Phys. Rev. Lett.* **2004**, *92*, 246401.
(74) Petachem. http://www.petachem.com (accessed April 28, 2016).
(75) Ufimtsev, I. S.; Martinez, T. J. Quantum Chemistry on Graphical Processing Units. 3. Analytical Energy Gradients, Geometry Optimization, and First Principles Molecular Dynamics. *J. Chem. Theory Comput.* **2009**, *5*, 2619−2628.
(76) Lee, C.; Yang, W.; Parr, R. G. Development of the Colle-Salvetti Correlation-Energy Formula into a Functional of the Electron Density. *Phys. Rev. B: Condens. Matter Mater. Phys.* **1988**, *37*, 785−789.
(77) Becke, A. D. Density-Functional Thermochemistry. Iii. The Role of Exact Exchange. *J. Chem. Phys.* **1993**, *98*, 5648−5652.
(78) Stephens, P. J.; Devlin, F. J.; Chabalowski, C. F.; Frisch, M. J. Ab Initio Calculation of Vibrational Absorption and Circular Dichroism Spectra Using Density Functional Force Fields. *J. Phys. Chem.* **1994**, *98*, 11623−11627.
(79) Vosko, S. H.; Wilk, L.; Nusair, M. Accurate Spin-Dependent Electron Liquid Correlation Energies for Local Spin Density Calculations: A Critical Analysis. *Can. J. Phys.* **1980**, *58*, 1200−1211.
(80) Hay, P. J.; Wadt, W. R. Ab Initio Effective Core Potentials for Molecular Calculations. Potentials for the Transition Metal Atoms Sc to Hg. *J. Chem. Phys.* **1985**, *82*, 270−283.
(81) Saunders, V. R.; Hillier, I. H. A "Level−Shifting" Method for Converging Closed Shell Hartree−Fock Wave Functions. *Int. J. Quantum Chem.* **1973**, *7*, 699−705.
(82) Rohrdanz, M. A.; Martins, K. M.; Herbert, J. M. A Long-Range-Corrected Density Functional That Performs Well for Both Ground-State Properties and Time-Dependent Density Functional Theory Excitation Energies, Including Charge-Transfer Excited States. *J. Chem. Phys.* **2009**, *130*, 054112.
(83) Klamt, A.; Schuurmann, G. Cosmo: A New Approach to Dielectric Screening in Solvents with Explicit Expressions for the Screening Energy and Its Gradient. *J. Chem. Soc., Perkin Trans. 2* **1993**, *2*, 799−805.
(84) Liu, F.; Luehr, N.; Kulik, H. J.; Martínez, T. J. Quantum Chemistry for Solvated Molecules on Graphical Processing Units Using Polarizable Continuum Models. *J. Chem. Theory Comput.* **2015**, *11*, 3131−3144.
(85) Bondi, A. Van Der Waals Volumes and Radii. *J. Phys. Chem.* **1964**, *68*, 441−451.
(86) Ioannidis, E. I.; Gani, T. Z. H.; Kulik, H. J. Molsimplify: A Toolkit for Automating Discovery in Inorganic Chemistry. *J. Comput. Chem.* **2016**, *37*, 2106−2117.
(87) Kästner, J.; Carr, J. M.; Keal, T. W.; Thiel, W.; Wander, A.; Sherwood, P. DL-FIND: An Open-Source Geometry Optimizer for Atomistic Simulations. *J. Phys. Chem. A* **2009**, *113*, 11856−11865.
(88) Boys, S. F.; Bernardi, F. d. The Calculation of Small Molecular Interactions by the Differences of Separate Total Energies. Some Procedures with Reduced Errors. *Mol. Phys.* **1970**, *19*, 553−566.
(89) Glendening, E. D.; Badenhoop, J. K.; Reed, A. E.; Carpenter, J. E.; Bohmann, J. A.; Morales, C. M.; Landis, C. R.; Weinhold, F. NBO, Version 6.0, 2013.
(90) Khaliullin, R. Z.; Cobar, E. A.; Lochan, R. C.; Bell, A. T.; Head-Gordon, M. Unravelling the Origin of Intermolecular Interactions Using Absolutely Localized Molecular Orbitals. *J. Phys. Chem. A* **2007**, *111*, 8753−8765.

DOI: 10.1021/acs.chemmater.6b02378
Chem. Mater. 2016, 28, 6207−6218

(91) Shao, Y.; Molnar, L. F.; Jung, Y.; Kussmann, J.; Ochsenfeld, C.; Brown, S. T.; Gilbert, A. T. B.; Slipchenko, L. V.; Levchenko, S. V.; O'Neill, D. P.; DiStasio, R. A., Jr; Lochan, R. C.; Wang, T.; Beran, G. J. O.; Besley, N. A.; Herbert, J. M.; Yeh Lin, C.; Van Voorhis, T.; Hung Chien, S.; Sodt, A.; Steele, R. P.; Rassolov, V. A.; Maslen, P. E.; Korambath, P. P.; Adamson, R. D.; Austin, B.; Baker, J.; Byrd, E. F. C.; Dachsel, H.; Doerksen, R. J.; Dreuw, A.; Dunietz, B. D.; Dutoi, A. D.; Furlani, T. R.; Gwaltney, S. R.; Heyden, A.; Hirata, S.; Hsu; Kedziora, G.; Khalliulin, R. Z.; Klunzinger, P.; Lee, A. M.; Lee, M. S.; Liang, W.; Lotan, I.; Nair, N.; Peters, B.; Proynov, E. I.; Pieniazek, P. A.; Min Rhee, Y.; Ritchie, J.; Rosta, E.; David Sherrill, C.; Simmonett, A. C.; Subotnik, J. E.; Lee Woodcock Iii, H.; Zhang, W.; Bell, A. T.; Chakraborty, A. K.; Chipman, D. M.; Keil, F. J.; Warshel, A.; Hehre, W. J.; Schaefer Iii, H. F.; Kong, J.; Krylov, A. I.; Gill, P. M. W.; Head-Gordon, M. Advances in Methods and Algorithms in a Modern Quantum Chemistry Program Package. *Phys. Chem. Chem. Phys.* **2006**, *8*, 3172−3191.
(92) Bader, R. F. A Quantum Theory of Molecular Structure and Its Applications. *Chem. Rev.* **1991**, *91*, 893−928.
(93) Lu, T.; Chen, F. Multiwfn: A Multifunctional Wavefunction Analyzer. *J. Comput. Chem.* **2012**, *33*, 580−592.
(94) Espinosa, E.; Molins, E.; Lecomte, C. Hydrogen Bond Strengths Revealed by Topological Analyses of Experimentally Observed Electron Densities. *Chem. Phys. Lett.* **1998**, *285*, 170−173.
(95) Noviandri, I.; Brown, K. N.; Fleming, D. S.; Gulyas, P. T.; Lay, P. A.; Masters, A. F.; Phillips, L. The Decamethylferrocenium/Decamethylferrocene Redox Couple: A Superior Redox Standard to the Ferrocenium/Ferrocene Redox Couple for Studying Solvent Effects on the Thermodynamics of Electron Transfer. *J. Phys. Chem. B* **1999**, *103*, 6713−6722.
(96) Forrow, N. J.; Sanghera, G. S.; Walters, S. J. The Influence of Structure in the Reaction of Electrochemically Generated Ferrocenium Derivatives with Reduced Glucose Oxidase. *J. Chem. Soc., Dalton Trans.* **2002**, 3187−3194.
(97) Atkins, P.; de Paula, J. *Atkins' Physical Chemistry*, 8th ed.; Oxford University Press, 2006.
(98) Grabowski, S. J. Ab Initio Calculations on Conventional and Unconventional Hydrogen Bonds-Study of the Hydrogen Bond Strength. *J. Phys. Chem. A* **2001**, *105*, 10739−10746.
(99) Grabowski, S. J. What Is the Covalency of Hydrogen Bonding? *Chem. Rev.* **2011**, *111*, 2597−2625.
(100) Gasparotto, P.; Ceriotti, M. Recognizing Molecular Patterns by Machine Learning: An Agnostic Structural Definition of the Hydrogen Bond. *J. Chem. Phys.* **2014**, *141*, 174110.
(101) Ashouri, M.; Maghari, A.; Karimi-Jafari, M. H. Hydrogen Bonding Motifs in a Hydroxy-Bisphosphonate Moiety: Revisiting the Problem of Hydrogen Bond Identification. *Phys. Chem. Chem. Phys.* **2015**, *17*, 13290−13300.
(102) Weinhold, F.; Klein, R. A. What Is a Hydrogen Bond? Resonance Covalency in the Supramolecular Domain. *Chem. Educ. Res. Pract.* **2014**, *15*, 276−285.
(103) Frenking, G.; Caramori, G. F. No Need for a Re-Examination of the Electrostatic Notation of the Hydrogen Bonding: A Comment. *Angew. Chem., Int. Ed.* **2015**, *54*, 2596−2599.
(104) Weinhold, F.; Klein, R. A. Improved General Understanding of the Hydrogen-Bonding Phenomena: A Reply. *Angew. Chem., Int. Ed.* **2015**, *54*, 2600−2602.
(105) Poater, J.; Fradera, X.; Sola, M.; Duran, M.; Simon, S. On the Electron-Pair Nature of the Hydrogen Bond in the Framework of the Atoms in Molecules Theory. *Chem. Phys. Lett.* **2003**, *369*, 248−255.
(106) Beer, P. D.; Gale, P. A.; Chen, G. Z. Electrochemical Molecular Recognition: Pathways between Complexation and Signalling. *J. Chem. Soc., Dalton Trans.* **1999**, 1897−1910.
(107) Smith, M. B.; March, J. *March's Advanced Organic Chemistry: Reactions, Mechanisms, and Structure*; John Wiley & Sons, 2007.
(108) Rodriguez, J.-G.; Oñate, A.; Martin-Villamil, R. M.; Fonseca, I. A Practical Synthesis of Ethynylferrocene from Ferrocene Carboxaldehyde: Structure of 1, 4-Diferrocenyl-1, 3-Butadiyne. *J. Organomet. Chem.* **1996**, *513*, 71−76.
(109) Kaserer, T.; Beck, K.; Akram, M.; Odermatt, A.; Schuster, D. Pharmacophore Models and Pharmacophore-Based Virtual Screening: Concepts and Applications Exemplified on Hydroxysteroid Dehydrogenases. *Molecules* **2015**, *20*, 22799−22832.
(110) Mao, X.; Tian, W.; Wu, J.; Rutledge, G. C.; Hatton, T. A. Electrochemically Responsive Heterogeneous Catalysis for Controlling Reaction Kinetics. *J. Am. Chem. Soc.* **2015**, *137*, 1348−1355.

DOI: 10.1021/acs.chemmater.6b02378
Chem. Mater. 2016, 28, 6207−6218